

# Joint Sensing, Communication, and AI: A Trifecta for Resilient THz User Experiences

Christina Chaccour, *Member, IEEE*, Walid Saad, *Fellow, IEEE*,  
Méroouane Debbah, *Fellow, IEEE*, and H. Vincent Poor, *Life Fellow, IEEE*

## Abstract

In this paper a novel joint sensing, communication, and artificial intelligence (AI) framework is proposed so as to optimize extended reality (XR) experiences over terahertz (THz) wireless systems. The proposed framework consists of three main components. *First*, a tensor decomposition framework is proposed to extract unique sensing parameters for XR users and their environment by exploiting then THz channel sparsity. Essentially, THz band's quasi-opticality is exploited and the sensing parameters are extracted from the uplink communication signal, thereby allowing for the use of the *same waveform, spectrum, and hardware for both communication and sensing functionalities*. Then, the Cramer-Rao lower bound is derived to assess the accuracy of the estimated sensing parameters. *Second*, a non-autoregressive multi-resolution generative artificial intelligence (AI) framework integrated with an adversarial transformer is proposed to predict missing and future sensing information. The proposed framework offers robust and comprehensive historical sensing information and anticipatory forecasts of future environmental changes, which are *generalizable to fluctuations in both known and unforeseen user behaviors and environmental conditions*. *Third*, a multi-agent deep recurrent hysteretic Q-neural network is developed to control the handover policy of reconfigurable intelligent surface (RIS) subarrays, leveraging the informative nature of sensing information to minimize handover cost, maximize the individual quality of personal experiences (QoPEs), and improve the robustness and resilience of THz links. Simulation results show a high generalizability of the proposed unsupervised generative AI framework to fluctuations in user behavior and velocity, leading to a 61 % improvement in instantaneous reliability compared to schemes with known channel state information.

## Index Terms

C. Chaccour and W. Saad are with the Wireless@VT, Bradley Department of Electrical and Computer Engineering, Virginia Tech, Arlington, VA, USA, Emails: christinac@vt.edu, walids@vt.edu.

M. Debbah is with the Technology Innovation Institute, 9639 Masdar City, Abu Dhabi, United Arab Emirates and also with CentraleSupélec, University Paris-Saclay, 91192 Gif-sur-Yvette, France, Email: merouane.debbah@tii.ae.

H.V. Poor is with Department of Electrical and Computer Engineering, Princeton University, NJ 08544, USA, Email: poor@princeton.edu.

extended reality (XR), terahertz (THz), artificial intelligence (AI), machine learning (ML), reliability, resilience, joint sensing and communications.

## I. INTRODUCTION

The sixth generation (6G) wireless system needs to support advanced services such as extended reality (XR)<sup>1</sup>, autonomous driving, and digital twins [1]. Catering to the demands of such applications requires wireless systems to not only provide communication services, but to also include sensing, localization, and control capabilities. In particular, designing a versatile wireless XR system that delivers a multi-sensory immersive experience poses numerous challenges, including the need to maximize data rates, ensure instant reliability, minimize latency, accurately track the six degrees of freedom (6DoF) of each XR user, and maintain situational awareness of the surrounding environment. One approach to overcoming these challenges involves the utilization of higher frequency bands, specifically the sub-terahertz (THz) and THz bands (0.1 – 10 THz), as they can provide significantly elevated data rates and high-resolution environmental sensing capabilities [2], which can culminate in a personalized and interactive experience. However, these bands, on their own, cannot fully resolve all the design challenges needed for a multi-sensory XR system experience, such as achieving instantaneous reliability, near-zero latency, and precise tracking of the 6DoF of each users' head and body.

THz networks could exploit the sensing information for two distinct key purposes: instilling sensing-driven *service* intelligence and sensing-driven *operational* intelligence. *First*, service intelligence refers to the ability of the XR system to accurately adapt and respond to the user's needs and preferences in real-time, based on the information gathered from each user's environment and interaction. For example, in VR, precise tracking of the user's movements and interactions is necessary to avoid motion sickness and other discomfort. In contrast, AR requires accurate tracking to maintain alignment between the real-world and the augmented environment. *On the other hand*, operational intelligence refers to the network's ability to sense the dynamic environment and incorporate its behavioral stochasticity in real-time. For instance, the narrow THz beams are particularly susceptible to minute changes induced by the user behavior and/or environment, necessitating frequent beam training and channel estimation. However, this approach results in significant overhead and delays, which are not acceptable

<sup>1</sup>XR encompasses augmented reality (AR), mixed reality (MR), and virtual reality (VR).

in wireless XR whose applications require *instantaneously continual high-rate THz beams* that guarantee seamless alignment between virtual and real environments. By leveraging sensing-driven operational intelligence, a THz network can effectively mitigate its intermittent link behavior and achieve a tight alignment between virtual and real environments, resulting in a seamless user experience. Additionally, by sharing the same waveform, hardware, and spectrum for communication and sensing functionalities, the system can form more robust beams in a time-critical manner, boosting spectral efficiency, and enhancing the user experience.

Fundamentally, the main goal of effective joint sensing and communication systems is to *mitigate every communication challenge and leverage it as a sensing opportunity*. Achieving this goal requires overcoming key challenges. *Firstly*, sensing and communication are functionally different<sup>2</sup>. Thus, there is a need for a holistic approach that can extract sensing parameters and analyze situational awareness from a wireless system designed to leverage the same waveform, spectrum, and hardware for both sensing and communication functions. *Secondly*, optimizing XR applications served by a THz network presents distinct challenges compared to traditional network optimization frameworks. Essentially, the inherently unpredictable nature of the THz channel requires *continual and complete sensing* input to ensure a resilient and seamless THz experience for XR users. Thus, it is necessary to leverage the sensing input for prediction and forecasting purposes so as to enable a *proactive* decision-making and adaptation to environmental dynamics, and ensure a resilient THz experience for XR users. *Thirdly*, putting the user and their quality of personal experience (QoPE) at the center is crucial to delivering personalized and immersive experiences in XR. This requires designing optimization frameworks that not only account for the diverse needs and preferences of different users but also adapt to the stochastic nature of the THz environment. Overall, these challenges require innovative solutions that can effectively address the resilience of THz links while exploiting the trifecta of sensing, communication, and AI faculties, and ultimately ensuring near-optimal immersive wireless XR experience.

#### A. Prior Works

The concept of joint communication and sensing has recently seen a surge of interest in the literature [4]–[8]. The work in [4] proposed a beamforming design dedicated for dual-

<sup>2</sup>For instance, sensing typically relies on unmodulated signals or short pulses and chirps. Communication signals, on the other hand, are a mix of unmodulated (pilots) and modulated signals [3].

functional radar and communication base stations. In [5], the authors exploited the potential of reconfigurable intelligent surfaces (RISs) to improve radar sensing in a non-orthogonal multiple access empowered integrated sensing and communication network. However, the works in [4] and [5] do not leverage the THz band’s quasi-opticality nor attempt to effectively mitigate the highly uncertain nature of the THz channel by capitalizing on the sensing input. Moreover, this prior art does not exploit the sensing functionality to improve the unique network performance indicators of wireless XR services. When it comes to THz sensing, the work in [6] considered the joint detection, mapping, and navigation problem by a drone with real-time learning capabilities. In [7], model-based and model-free hybrid beamforming techniques are proposed for a joint radar and communication system. The authors in [8] developed a joint reference signal and synchronization signal block-based sensing scheme to predict the need for beam switches. Nonetheless, these works [4]–[8] do not opportunistically use the same spectrum, waveform, and hardware at THz bands for joint sensing and communications. Consequently, these existing deployment strategies lead to higher costs in terms of hardware and resources, which is not suitable for commercial XR services. In [9], we proposed a novel joint sensing and communication system that utilizes the same waveform, hardware, and spectrum. However, our work in [9] does not have the AI capabilities needed to predict missing and future sensing information. In fact, our prior work mainly relies on the sensing input in its raw unoptimal structure. In particular, and more importantly, the works in [4]–[9] do not design robust and resilient AI-oriented frameworks that can optimize the *instantaneous* user experience of future user-centric and intelligence-centric 6G applications. Clearly, the current body of literature on joint sensing and communication systems at THz frequencies lacks a comprehensive and foundational approach to adequately address the challenge of managing uncertainty in THz channels through the integration of AI and sensing.

### B. Contributions

The main contribution of this paper is, thus, a novel design, analysis, and optimization framework that integrates communication, sensing, and AI, to address the fundamental question of whether or not such integrated systems can provide highly reliable THz links instantaneously. If this is not the case, *can such systems still deliver robust and resilient THz experiences to XR users?* Fig. 1 illustrates the roadmap of our approach, with our key contributions being:

- To extract the environmental *sensing* parameters that characterize the DoF and associated blockages of wireless XR users, we leverage the THz uplink *communication* waveform via

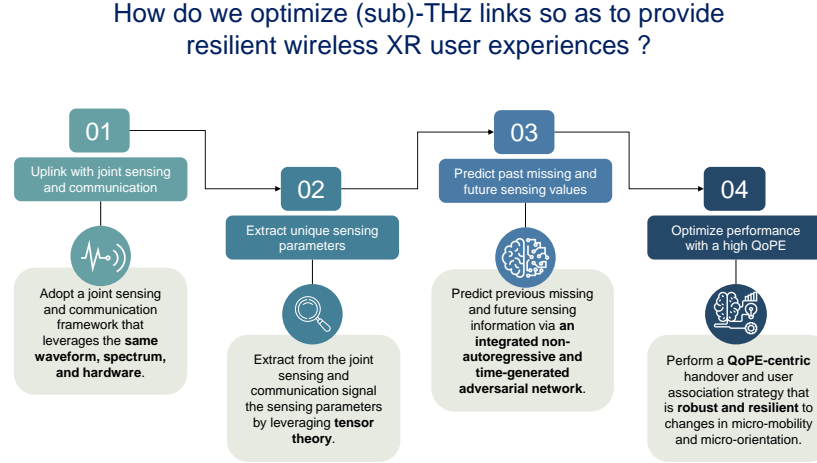


Fig. 1: Illustrative figure showcasing the key steps to optimize the QoPE of XR users served with THz links.

tensor theory. In particular, we improve the spectral and energy efficiency of our design by opportunistically utilizing the same waveform, hardware, and spectrum for sensing and communication. We also leverage the inherent sparsity in the THz bands to perform a tensor decomposition of the received uplink signal, and we prove the uniqueness of our extracted sensing parameters.

- To assess the accuracy of our estimated sensing parameters, we derive their Cramér–Rao lower bound (CRLB) and analyze the parameters that may affect the variability of the estimation. Our derived results show that the estimation error varies non-monotonically with the carrier frequencies, i.e., frequencies above 1 THz exhibit higher molecular absorption lines. This underscores the significance of operating within the sub-THz spectrum, as it achieves a favorable equilibrium between the inherent tradeoffs of sensing and communication functionalities.
- To address the issue of missing tracking and blockage sensing information caused by the intermittent nature of links, we propose a novel AI-based imputation design that exploits a novel non-autoregressive multi-resolution generative framework to predict the missing values in a sequence of sensing values. We then propose a novel adversarial transformer framework that processes comprehensive sensing information and then, predicts, future user behavior and dynamic changes to the environment (e.g. potential blockages). These designs enable the recovery of missing tracking and blockage sensing information thus allowing the network to anticipate user behavior, ensuring *seamless, continual, and uninterrupted XR*

*experiences.*

- We then introduce a novel QoPE-centric-aware optimization problem that leverages the designed sensing and communication capabilities to optimize handover– a challenging task in a highly uncertain, dynamic network that relies narrow beamwidths. This approach accounts for both current and anticipated user behavior, and allows minimization of the frequency of unnecessary handovers thereby ensuring the robustness and resilience of THz links. To address this problem, we introduce a semi-distributed multi-agent reinforcement learning (RL) framework that substantially improves the resilience of individualized user experiences across the entire XR spectrum through its tailored reward system.
- Simulation results demonstrate that the proposed integrated imputation-forecasting system has higher generalizability and maintains accuracy despite fluctuations in user speed and number of users entering/leaving the room, while vanilla deep learning frameworks quickly lose accuracy. The QoPE-centric optimization framework significantly improves user reliability and resilience, with gains of up to 78 % compared to baseline schemes with known channel state information (CSI) and beam tracking.

## II. SYSTEM MODEL

Consider the downlink and uplink of an RIS-based single cell-THz system operating as a joint sensing and communication system in a confined indoor area. A set  $\mathcal{B}$  of  $B$  RISs are used as THz base stations (BSs) that transmit XR content and provide situational awareness for a set  $\mathcal{U}$  of  $U$  mobile wireless XR users. Each subarray  $n$  of RIS  $b$  in  $\mathcal{B}$  is located at  $\mathbf{l}^{b,n} = [l_x^{b,n}, l_y^{b,n}]^T \in \mathbb{R}^2$ . The XR users are mobile and may change their locations and orientations at any point in time. As such,  $\mathbf{l}^u = [l_x^u, l_y^u]^T \in \mathbb{R}^2$  denotes the position of user  $u$ . Here, *situational awareness* refers to the process of mapping the physical world, including the location, orientation, and state of physical objects, to the digital realm with a certain level of accuracy. We consider the *entire XR reality-virtuality continuum*, as will be evident in our later analysis. RISs are used to provide nearly continuous line-of-sight (LoS) data links to the XR users. This RIS-enhanced architecture also creates multiple independent paths capable of gathering rich information about the environment [3]. Each RIS consists of a two-dimensional large antenna array that has an array of subarray (AoSA) structure [10]. Antenna elements of the same subarray are connected to the same phase shifter and radio frequency (RF) chain, thus reducing the number of phase shifters needed compared to a fully-connected array structure. Each subarray has a large number of antennas  $M$

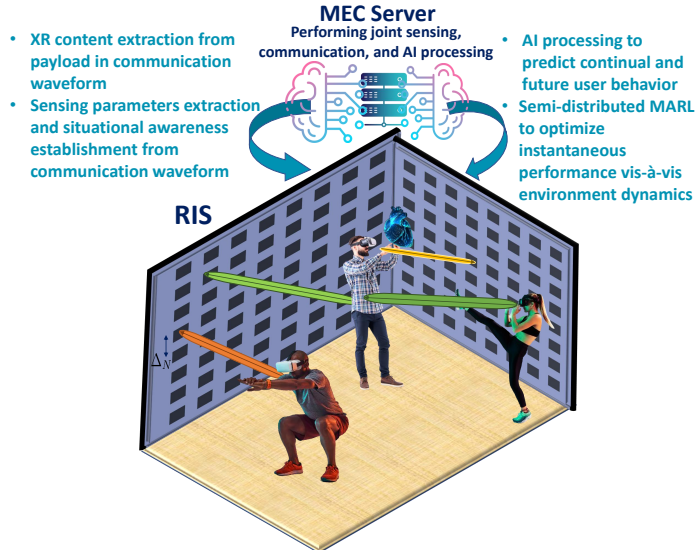


Fig. 2: Illustrative example of our THz-based wireless XR system for joint communication, sensing, and AI.

and the spacing between antenna elements within each RIS subarray is  $\delta_m$ . The total number of subarrays is  $N$  with the spacing between them being  $\Delta_N$ . These subarrays collectively employ a hybrid beamforming architecture. Without loss of generality, we assume  $N \geq U$ , thus providing XR users with sufficient DoF in terms of association. This subarray structure allows us to have  $N$  independent channels each RIS.

#### A. Joint Communication and Sensing Model

Consider an arbitrary RIS in  $\mathcal{B}$  that captures the situational awareness and mapping information, and receives high data rate XR content as in Fig. 2. We assume that the RIS has performed synchronization and initial beam alignment according to existing techniques (e.g. [11]). To maintain high-resolution real-time user tracking and a situational awareness of the indoor area, each RIS will continuously collect a sequence of  $T$  snapshots of the received uplink communication signal that are then used to estimate and track the angle of arrival (AoA), angle of departure (AoD), and time of arrival (ToA) of users as well as the location of obstacles leading to non-line-of-sight (NLoS) communications. Since we use indoor RISs, blockages mostly occur due to bodies of the users.

Each XR user has a uniform linear array (ULA) of  $Q$  antennas and  $R$  RF chains. Hence, if all XR users are active,  $U$  data signaling beams are sent simultaneously to the RIS. To mitigate the high peak to average power ratio (PAPR) effect of orthogonal frequency-division

multiplexing (OFDM) schemes, a single carrier frequency-division multiplexing (SC-FDM) is used to maintain high energy efficiency at the user equipment. The far-field electromagnetic (EM) wave condition is assumed to be met. After beamforming, the transmitted user signal at subcarrier  $k$  is  $\mathbf{s}_k(t) = \mathbf{F}_R(t)\mathbf{F}_k(t)\mathbf{x}_k(t), \forall k = 1, \dots, K$ , where  $\mathbf{x}_k(t) \in \mathbb{C}^{L \times 1}$  is the transmitted uplink communication signal,  $\mathbf{F}_k \in \mathbb{C}^{R \times l}$  is the digital precoding matrix for subcarrier  $k$ , and  $\mathbf{F}_R(t) \in \mathbb{C}^{Q \times R}$  is the RF precoder for all subcarriers. After processing the communication waveform of subcarrier  $k$ , the uplink received signal at each RIS subarray  $n$  will be  $y_{n,k}(t) = \mathbf{w}_{n,k}^T \mathbf{H}_{n,u}^k(t) \mathbf{s}_k(t) + \nu_{n,k}(t)$ , where  $\mathbf{w}_{n,k} \in \mathbb{C}^{M \times 1}$  is the combining vector of RIS subarray  $n$  at subcarrier  $k$ ,  $\mathbf{H}_{n,u}^k \in \mathbb{C}^{M \times Q}$  is the uplink channel matrix for subcarrier  $k$ , and  $\nu_{n,k} \sim \mathcal{CN}(\mathbf{0}, \mathbf{I}_{M \times Q})$  is the additive Gaussian noise vector at subarray  $n$  and subcarrier  $k$ . To construct a single realization for sensing the wireless environment,  $T$  snapshots are recorded by the RIS, each of which captures  $J$  uplink measurements:

$$\mathbf{y}_{n,k}(t) = \mathbf{W}_{n,k}^T \mathbf{H}_{n,u}^k(t) \mathbf{F}_R^m(t) \mathbf{F}_k(t) \mathbf{s}_k(t) + \boldsymbol{\nu}_{n,k}(t), \quad (1)$$

where  $\mathbf{y}_{n,k}(t) \triangleq [y_{n,k,1}(t) \dots y_{n,k,J}(t)]^T$ ,  $\boldsymbol{\nu}_{n,k}(t) \triangleq [\nu_{n,k,1}(t) \dots \nu_{n,k,J}(t)]^T$ ,  $\mathbf{W}_{n,k} \triangleq [\mathbf{w}_{n,k,1} \dots \mathbf{w}_{n,k,J}]$ .

The  $M \times Q$  multiple-input multiple-output (MIMO) channel matrix between user  $u$  and RIS subarray  $n$  in the time domain is:  $\mathbf{H}_{n,u}(t) = \sum_{p=1}^P \alpha_{n,u}^p \mathbf{a}_r(\phi_{n,u}^p) \mathbf{a}_t^H(\theta_{n,u}^p) \delta(t - \tau_{n,u})$ , where  $(\cdot)^H$  is the conjugate transpose,  $\alpha_{n,u}^p \in \mathbb{C}$  is the complex channel gain,  $P$  is the number of distinct spatial paths,  $\theta_{n,u}^l$  is the AoD of path  $p$  of antenna  $u$ ,  $\tau_{n,u}$  is the ToA, and  $\phi_{n,u}^p$  is the AoA of path  $p$  at subarray  $n$ . The array steering vector of the antenna array of the XR user and the RIS subarray, have a ULA structure<sup>3</sup>, and are given by:  $\mathbf{a}_t(\theta_{n,u}^p) = \frac{1}{\sqrt{Q}} \left[ 1, e^{j \frac{2\pi}{\delta_m} \sin(\theta_{n,u}^p)}, \dots, e^{j(Q-1) \frac{2\pi}{\delta_m} \sin(\theta_{n,u}^p)} \right]^T$ ,  $\mathbf{a}_r(\phi_{n,u}^p) = \frac{1}{\sqrt{M}} \left[ 1, e^{j \frac{2\pi}{\delta_m} \sin(\phi_{n,u}^p)}, \dots, e^{j(M-1) \frac{2\pi}{\delta_m} \sin(\phi_{n,u}^p)} \right]^T$ . Consequently, the channel matrix in the frequency domain associated with subcarrier  $k$  will be:

$$\mathbf{H}_{n,u}^k(f) = \sum_{p=1}^P \alpha_{n,u}^p \mathbf{a}_r(\phi_{n,u}^p) \mathbf{a}_t^H(\theta_{n,u}^p) \exp\left(-\frac{j2\pi f \tau_{n,u}}{K}\right). \quad (2)$$

The snapshots in (1) can be collected over line-of-sight (LoS) or NLoS communication signal waveforms. For the LoS, the uplink channel gain will be [12]:  $\alpha_{n,u}^L = \frac{c}{4\pi f r_{n,u}} e^{-\frac{k(f)r_{n,u}}{2}} e^{-j2\pi f \tau_{n,u}^L}$ . Here,  $c$  is the speed of light,  $k(f)$  is the overall molecular absorption coefficients of the medium at THz band,  $f$  is the operating frequency, and  $r_{n,u}$  is the distance between XR user  $u$  and RIS subarray  $n$ . From this channel gain, we can see that, for LoS conditions, the parameters to be

<sup>3</sup>While uniform planar arrays can be used for our 2D subarrays, we adopt ULA for analytical tractability.



estimated are  $\{\theta_{n,u}^L, \phi_{n,u}^L, \tau_{n,u}^L\}$ . This process allows tracking XR users in real-time. Here, we do not consider NLoS links for communications purposes due to the poor propagation characteristics of THz signals (e.g., limited reflection) and their high susceptibility to blockage. In other words, the NLoS link cannot meet the high-rate XR needs. Nonetheless, from a sensing standpoint, instead of discarding the NLoS signal completely, we use it to track the user and gather a situational awareness of the blockage incidence. In NLoS conditions, the channel gain is given by [13]:  $\alpha_{n,u}^N = \frac{c}{4\pi f(r_{n,u}^{(1)} + r_{n,u}^{(2)})} e^{\left(-\frac{k(f)(r_{n,u}^{(1)} + r_{n,u}^{(2)})}{2}\right)} R(f) e^{-j2\pi f \tau_{n,u}^N}$ , where  $r_{n,u}^{(1)}$  is the distance between the XR user  $u$  and the reflecting point, and  $r_{n,u}^{(2)}$  is the distance between the reflecting point and RIS subarray  $n$ . For reflections, we consider the transverse electric part of the EM wave, i.e., the signal is assumed to be perpendicular to the plane of incidence. This assumption is valid given the placement of our RIS per Fig. 2. Thus,  $R_{n,u}(f) = \gamma_{n,u}(f)\rho_{n,u}(f)$ , is the reflection coefficient, where  $\gamma(f) \approx -\exp\left(\frac{-2\cos(\psi_{n,u})}{\sqrt{\eta(f)^2 - 1}}\right)$  is the Fresnel reflection coefficient and  $\rho_{n,u}(f) = \exp\left(-\frac{8\pi^2 f^2 \sigma^2 \cos^2(\psi_{n,u})}{c^2}\right)$  is the Rayleigh factor that characterizes the roughness effect.  $\psi_{n,u}$  is the angle of the incident signal to the reflector,  $\eta(f)$  is the refractive index, and  $\sigma$  is the surface height standard deviation. Thus, for NLoS, the parameters to be estimated are:  $\{\theta_{n,u}^N, \phi_{n,u}^N, \tau_{n,u}^N, \psi_{n,u}\}$ . Next, we formulate the problem of estimating the sensing parameters from the  $T$  collected snapshots in (1). To do so, we leverage the sparsity of the THz channel matrix and reformulate the received uplink signal expression as a tensor.

### III. SITUATIONAL AWARENESS ESTIMATION VIA TENSOR DECOMPOSITION

#### A. Problem Formulation

Estimating the sensing parameters from  $T$  communication snapshots recorded at the RIS subarray faces multiple challenges. First, existing estimation techniques [14]–[16] rely on the collection of pilot signals and their goal is to estimate the channel. In contrast, our goal here is to collect uplink communication signals used by users during an XR session so as to *continuously track* the sensing parameters.<sup>4</sup> Second, existing parameter estimation methods [17]–[19] have their own limitations: Off-grid methods like multiple signal classification (MUSIC) cannot jointly estimate multiple sensing parameters, leading to a difficult pairing problem [18]. Also, the MUSIC algorithm cannot be readily applied to the peculiar AoSA structure of hybrid THz beamforming as its complexity of the method becomes impractical with large antenna arrays

<sup>4</sup>Communication was initiated after a successful initial access and beam alignment prior to the XR session.

[17]. Moreover, on-grid methods like compressive sensing [19] are constrained by their grid spacing, which increases complexity if a high-resolution is desired.

To successfully estimate the THz sensing parameters, we concatenate  $T$  snapshots of the received uplink signal:

$$\begin{aligned} \mathbf{Y}_{n,k} &= \mathbf{W}_{n,k}^T \mathbf{H}_{n,u}^k(f) \boldsymbol{\Omega} + \mathbf{N}_{n,k}, \\ \mathbf{Y}_{n,k} &\triangleq \begin{bmatrix} \mathbf{y}_{n,k}(1) & \dots & \mathbf{y}_{n,k}(T) \end{bmatrix}, \mathbf{N}_{n,k} \triangleq \begin{bmatrix} \boldsymbol{\nu}_{n,k}(1) & \dots & \boldsymbol{\nu}_{n,k}(T) \end{bmatrix}, \\ \boldsymbol{\Omega} &\triangleq \begin{bmatrix} \mathbf{F}_R^m(1) \mathbf{F}_k(1) \mathbf{s}_k(1) & \dots & \mathbf{F}_R^m(T) \mathbf{F}_k(T) \mathbf{s}_k(T) \end{bmatrix}. \end{aligned} \quad (3)$$

From (3), we observe that the received signal has three modes that represent the number of measurements, the number of snapshots, and the number of subcarriers, respectively. Thus, we can model it as a three-order tensor, namely,  $\boldsymbol{\chi} \in \mathbb{C}^{J \times T \times K}$ . In fact, substituting (2) in (3) yields:

$$\mathbf{Y}_{n,k}(t) = \sum_{p=1}^P \Lambda_{n,u,k}^p \zeta(\phi_{n,u}^p) \boldsymbol{\xi}(\theta_{n,u}^p)^H + \mathbf{N}_{n,k}. \quad (4)$$

In (4),  $\Lambda_{n,u,k}^p \triangleq \alpha_{n,u}^p \exp\left(-\frac{j2\pi f \tau_{n,u}}{K}\right)$ ,  $\zeta_k(\phi_{n,u}^p) \triangleq \mathbf{W}_{n,k}^T \mathbf{a}_r(\phi_{n,u}^p)$ , and  $\boldsymbol{\xi}_k(\theta_{n,u}^p) \triangleq \boldsymbol{\Omega}^H \mathbf{a}_t(\theta_{n,u}^p)$ . Clearly, each slice  $\mathbf{Y}_{n,k}$  corresponding with tensor  $\boldsymbol{\chi}$  is a weighted sum of a common set of rank-one outer products. Hence, we can factorize the tensor as follows:

$$\boldsymbol{\chi} = \sum_{p=1}^P \zeta_k(\phi_{n,u}^p) \circ \boldsymbol{\xi}_k(\theta_{n,u}^p) \circ \Lambda_{n,u}^p + \mathcal{W} = [[\mathbf{A}, \mathbf{B}, \mathbf{C}]] + \mathcal{W},$$

$$\mathbf{A} \triangleq \begin{bmatrix} \zeta_1(\phi_{n,u}^1) & \dots & \zeta_K(\phi_{n,u}^1) \end{bmatrix}, \mathbf{B} \triangleq \begin{bmatrix} \boldsymbol{\xi}_1(\theta_{n,u}^1) & \dots & \boldsymbol{\xi}_K(\theta_{n,u}^1) \end{bmatrix}, \mathbf{C} \triangleq \begin{bmatrix} \Lambda_{n,u,1}^1 & \dots & \Lambda_{n,u,K}^1 \end{bmatrix}. \quad (5)$$

Here,  $\circ$  is the outer product symbol,  $\Lambda_{n,u,k}^p = \left\{ \alpha_{n,u}^p \exp\left(-\frac{j2\pi f \tau_{n,u}}{K}\right) \right\}_{t=1}^T$ , and  $\mathcal{W}$  is  $\mathbf{N}_{n,k}$  in the tensor domain.  $\mathbf{A}$ ,  $\mathbf{B}$ , and  $\mathbf{C}$  are the three factor matrices associated to the tensor  $\boldsymbol{\chi}$ . We note that, the sparsity of the THz channel and the limited number of propagation paths, leveraging tensor theory is particularly efficient and can guarantee the uniqueness of the estimated sensing parameters. Moreover, our approach can characterize the sensing parameters from the collected snapshots without imposing additional constraints or assumptions. For instance, alternatively adopting matrix factorization almost never leads to a unique solution unless the rank of the matrix is one or further conditions are imposed on the factor matrices.

### B. Proposed Sensing Parameters Estimation Method

After factorizing the tensor  $\boldsymbol{\chi}$ , extracting the sensing parameters and estimating them requires solving the following optimization problem:

$$\min_{\tilde{\mathbf{A}}, \tilde{\mathbf{B}}, \tilde{\mathbf{C}}} \left\| \boldsymbol{\chi} - \sum_{p=1}^P \tilde{\mathbf{a}}_p \circ \tilde{\mathbf{b}}_p \circ \tilde{\mathbf{c}}_p \right\|_F^2, \quad (6)$$

where  $\tilde{\mathbf{A}} = [\tilde{\mathbf{a}}_1 \cdots \tilde{\mathbf{a}}_P]$ ,  $\tilde{\mathbf{B}} = [\tilde{\mathbf{b}}_1 \cdots \tilde{\mathbf{b}}_P]$ ,  $\tilde{\mathbf{C}} = [\tilde{\mathbf{c}}_1 \cdots \tilde{\mathbf{c}}_P]$  are the three estimated factor matrices. To solve this problem, the three factor matrices need to be estimated. To do so, we leverage the sparsity of the THz channel that guarantees the uniqueness condition for tensor decomposition. This allows us to establish a relationship between the true factor matrices and their estimates. Thus, given these relationships, we next derive the environmental sensing parameters.

**Theorem 1:** The AoA, AoD, and ToA corresponding to path  $p$  between RIS subarray  $n$  and user  $u$  are:

$$\tilde{\phi}_{n,u}^P = \arg \max_{\phi_{n,u}^P} \frac{|\tilde{\mathbf{a}}_k^H \tilde{\boldsymbol{\zeta}}_k(\phi_{n,u}^P)|}{\|\tilde{\mathbf{a}}_k\|_2 \|\tilde{\boldsymbol{\zeta}}_k(\phi_{n,u}^P)\|_2}, \quad (7)$$

$$\tilde{\theta}_{n,u}^P = \arg \max_{\theta_{n,u}^P} \frac{|\tilde{\mathbf{b}}_k^H \tilde{\boldsymbol{\xi}}_k(\theta_{n,u}^P)|}{\|\tilde{\mathbf{b}}_k\|_2 \|\tilde{\boldsymbol{\xi}}_k(\theta_{n,u}^P)\|_2}, \quad (8)$$

$$\tilde{\tau}_{n,u}^P = \arg \min_{\tau_{n,u}^P} \frac{|\tilde{\mathbf{c}}_k^H \tilde{\boldsymbol{\Lambda}}_{n,u,k}^P(\theta_{n,u}^P)|}{\|\tilde{\mathbf{c}}_k\|_2 \|\tilde{\boldsymbol{\Lambda}}_{n,u,k}^P(\tau_{n,u}^P)\|_2}. \quad (9)$$

*Proof:* See Appendix A ■

(7)-(9) can be solved with a one-dimensional search. Thus, the estimated AoA, AoD, and ToA allow us to track the XR user in near real-time. After obtaining  $\tilde{\phi}_{n,u}^P$ ,  $\tilde{\theta}_{n,u}^P$ , and  $\tilde{\tau}_{n,u}^P$ , the attenuation factor  $\alpha_{n,u}^P$  can be obtained by substitution. To determine the tracking information of the user and the blockers, we use our approach in Algorithm 1 in [9], which enables the RIS characterize the spatial availability of communications.

### C. Uniqueness and Accuracy of Estimated Sensing Parameters

We now further analyze our tensor decomposition technique and our estimated sensing parameters. The accuracy and precision of our estimations play a fundamental role for the service needs of the XR application and the THz system performance. For example, in VR, a precise tracking of the user's head and body movements is essential for creating a fully immersive experience. Meanwhile, in AR, an accurate registration of virtual objects onto the real-world scene is crucial for providing an uninterrupted and continuous experience. Next, we prove that our obtained sensing parameters are unique. Then, we capture the accuracy of the sensing parameters via the CRLB which is a fundamental theoretical limit on the precision of any unbiased estimator [20] that also provides a measure of the minimum achievable variance in the estimation of a sensing parameter. Thus, knowing the CRLB enables us to determine the accuracy and the sensitivity of our tensor decomposition mechanism in identifying the sensing parameters.

1) *Uniqueness of Sensing Parameters:* Achieving uniqueness in sensing parameters is essential in the Candecomp/Parafac (CP) decomposition-based method, which relies on Kruskal's condition [21]. Next, we prove the uniqueness of our solution.

**Lemma 1:** The XR user's estimated tracking parameters, obtained at LoS,  $\{\tilde{\phi}^L, \tilde{\theta}^L, \tilde{\tau}^L\}$ , and the blocker's estimated sensing parameters, obtained at NLoS,  $\{\tilde{\phi}^N, \tilde{\theta}^N, \tilde{\tau}^N\}$  are guaranteed to be unique because of the sparsity of the THz channel.

*Proof:* See Appendix B ■

2) *CRLB of Sensing Parameters:* We now derive the CRLB as follows:

**Proposition 1:** The CRLB of the XR users sensing parameters at LoS and NLoS is given by:

$$\text{CRLB}(\mathbf{S}^P) = \left[ \mathbb{E} \left\{ \left( \frac{\partial L(\mathbf{S}^P)}{\partial \mathbf{S}^P} \right)^H \left( \frac{\partial L(\mathbf{S}^P)}{\partial \mathbf{p}} \right) \right\} \right]^{-1}, \quad (10)$$

where  $\mathbf{S}^P$  is the vector of sensing parameters, and  $L(\mathbf{S}^P) = -JTK \log(\pi\sigma_{\mathcal{W}}) - \frac{1}{\sigma_{\mathcal{W}}} \|\mathbf{Y}_{(1)}^T - (C \odot B)A^T\|_F$  is the log-likelihood of  $\mathbf{S}^P$ . Here,  $Y_{(1)}$  is the mode-1 unfolding of  $\chi$  and  $\sigma_{\mathcal{W}}$  is the total noise standard deviation in the tensor domain.

*Proof:* The proof builds on [20], [22]–[24], and is omitted due to space constraints. ■

From Proposition 1, one can see that our estimation is mainly driven by the noise of the channel. Interestingly, given that we are operating at THz bands, the total noise power is the sum of the molecular absorption noise and the Johnson-Nyquist noise generated by the thermal agitation of electrons in conductors. Thus, while sensing at higher carrier frequencies and larger bandwidths may achieve higher resolutions, *the molecular absorption noise at higher carrier frequencies will affect the accuracy of the estimated sensing parameters.* With higher resolutions, it is necessary to control the variance of the estimates to considerably lower bounds<sup>5</sup>. Hence, there exists a *duality between communication and sensing as we go to higher carrier frequencies.* Thus, the operation at *sub-THz* bands is increasingly appealing as it could provide high data rates and high-resolution sensing while circumventing the inherent unreliability of higher frequencies, which are further compromised by molecular absorption losses.

#### IV. PREDICTING CONTINUAL AND FUTURE USER BEHAVIOR VIA GENERATIVE AI

Thus far, we have used tensor theory to analyze the received signal strength and extract the tracking parameters for LoS links, and the mapping information for NLoS links. Nonetheless, our

<sup>5</sup>For instance, when the sensing parameters have a resolution in the centimeter range, the variance should be in the millimeter or micrometer range.

sensing information from Section III is not comprehensive and is dependent on the user's alignment with the subarray. For instance, when all users are in perfect LoS with their corresponding subarray, our Section III measurements cannot characterize the possibility of blockage that may or may not occur. Similarly, if a particular user is in NLoS, our tensor-driven approach alone cannot enable tracking the user's DoF during these time slots. As a result, we would not be able to assess the *comprehensive and continual user behavior and environment dynamics*. One could argue that such gaps in user behavior and environment dynamics can be found via *averaging*, nonetheless, the stringent requirements of XR services impose a degree of immersion which requires sensing information to be available *instantaneously and continuously*. Here, we will first propose a novel non-autoregressive approach to predict the missing values of LoS and NLoS sensing matrices, namely *our imputation system*<sup>6</sup>. Then, we use these comprehensive time-variant vectors to predict future time slots via an encoder-decoder transformed based generative AI framework. To the best of our knowledge, this is the first work that combines both imputation and forecasting systems in a single framework. This novel integration offers a significant advantage over existing methods by providing a more accurate and generalizable prediction of future time slots based on continuous and comprehensive sensing data. As will be evident later, such future user behavior predictions will enable us to control the uncertainty of the THz channel, improve the overall performance instantaneously, and will enable the user *experience to be resilient*. Note that these predictions are not predicting the proper LoS and NLoS values for the time-slots with missing or future values. Instead, they provide RIS-operated BSs instantaneous and continual information about the users' behavior and their corresponding varying environments. Thus, this end-to-end (E2E) imputation-forecasting learning framework enables us to obtain a comprehensive sensing cognizance in terms of tracking and situational awareness.

#### A. Continual Prediction of User Behavior and Environmental Dynamics via Non-Autoregressive Multi-Resolution Generation

Consider the link between user  $u$  and RIS subarray  $n$ . To simplify the notation, we omit subscripts  $u$  and  $n$ . Let  $\mathbf{S}^L = (\mathbf{S}_1^L, \mathbf{S}_2^L, \dots, \mathbf{S}_T^L)$  be the sequence of  $T$  snapshots of LoS sensing information, whereby  $\mathbf{S}_i^L = [\tilde{\phi}^L, \tilde{\theta}^L, \tilde{\tau}^L]^T$ . We also define  $\mathbf{S}^N = (\mathbf{S}_1^N, \mathbf{S}_2^N, \dots, \mathbf{S}_T^N)$

<sup>6</sup>Imputation refers to the ability to intelligently recover and predict missing sequential sensing values to obtain a continuous and instantaneous sensing vector versus time.

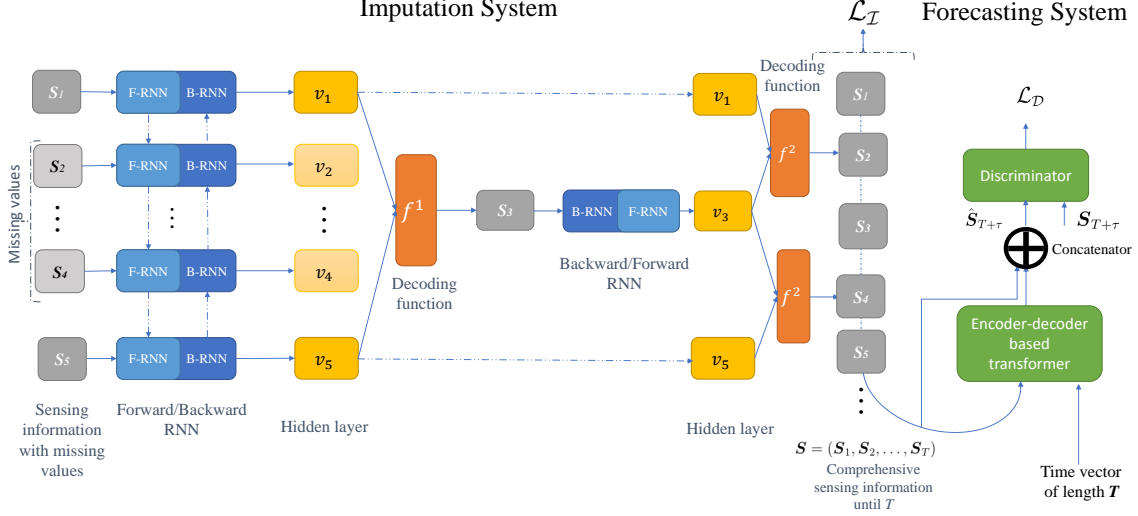


Fig. 3: Illustrative figure showcasing: A) The non-autoregressive multi-resolution imputation approach for predicting missing sensing information. For illustrative purposes the figure, we show a sequence of five sensing values, that include three missing values. B) The forecasting approach via an adversarial sparse transformer model.

as the sequence of snapshots of NLoS whereby  $\mathbf{S}_i^N = [\tilde{\phi}^N, \tilde{\theta}^N, \tilde{\tau}^N]^T$ . These values represent captured sensing information that characterizes the behavior of users and their corresponding dynamic time-varying environment. However, such vectors contain missing values due to beam misalignments and the intermittent nature of THz links. Our goal is to characterize the *continual and fine-grained* behavior of users and the time varying environment in these gaps, produced by beam misalignments, by predicting the missing values of  $\mathbf{S}^L$  and  $\mathbf{S}^N$ . The missing values in  $\mathbf{S}^L$  are captured by a masking sequence  $\Xi^L = (\Xi_1^L, \Xi_2^L, \dots, \Xi_T^L)$ , while the missing values in  $\mathbf{S}^N$  are found by its complement masking sequence  $\Xi^N$ . Thus, when the user is in LoS,  $\Xi_i^L = [1, 1, 1]^T$  and  $\Xi_i^N = [0, 0, 0]^T$ . In contrast, in NLoS, we have  $\Xi_i^L = [0, 0, 0]^T$  and  $\Xi_i^N = [1, 1, 1]^T$ . We also define  $p(\mathbf{S}_1^L, \dots, \mathbf{S}_T^L) = \prod_t p(\mathbf{S}_t^L | \mathbf{S}_{<t}^L)$ . To factorize this probability, one can use the chain rule and train a deep autoregressive model for imputation as in [25]. Nonetheless, autoregressive models perform this task using sub-optimal values when attempting to search the missing values and are susceptible to error compounding for sequences with a long range. Such autoregressive models assume that the current value of a time series is a function of its past values. As the length of the sequence increases, the number of required past values also increases, resulting in a very large number of parameters to estimate. Since we want to capture fine-grained sensing information, our measurements can consist of long sequences

which can lead to overfitting and poor performance in capturing long-term dependencies. This creates a mismatch between the imputed sensing information that we must predict and the actual, observed indoor dynamics. To address these challenges, we propose a novel joint non-autoregressive generative and adversarial approach, whereby a deep non-autoregressive multi-resolution generative model [25] is used to recover missing observational sensing information. Meanwhile, an encoder-decoder based transformer [26] uses the new continual predicted sensing information to predict future information.

The architecture of this deep non-autoregressive, multi-resolution, generative model [25] consists of two components: a) a forward-backward encoder that maps the incomplete sequences of LoS and NLoS sensing sequences into hidden representations, and b) a multi-resolution decoder that imputes the missing values of LoS given the hidden representations constructed in a).

1) *Forward-backward encoder to represent missing sensing information:* Every  $\mathbf{S}^L$ ,  $\mathbf{S}^N$  and its corresponding mask  $\Xi^L$  and  $\Xi^N$  are concatenated as  $\Theta^L = [\mathbf{S}^L, \Xi^L]$ , and  $\Theta^N = [\mathbf{S}^N, \Xi^N]$ . The LoS and NLoS sensing information will undergo an encoder, which models a conditional distribution of two sets of hidden states given the sensing and masked input. We define  $\Upsilon^{F,L} = (v_1^{F,L}, \dots, v_T^{F,L})$  and  $\Upsilon^{F,N} = (v_1^{F,N}, \dots, v_T^{F,N})$  as the forward hidden states as well as  $\Upsilon^{G,L} = (v_1^{G,L}, \dots, v_T^{G,L})$  as the backward hidden states. Subsequently, the conditional probability distribution functions will be:

$$p(\Upsilon^{F,P}|\Theta^P) = \prod_{t=1}^T p(v_t^{F,P}|v_{<t}^{F,P}, \Theta_{\leq t}^P), \quad p(\Upsilon^{G,P}|\Theta^P) = \prod_{t=1}^T p(v_t^{G,P}|v_{>t}^{G,P}, \Theta_{\geq t}^P), \quad (11)$$

where  $P = \{L, N\}$  indicates the LoS or NLoS path. In (11), we can see that the product of distributions can be parametrized via a forward and backward recurrent neural network (RNN).

2) *Multi-resolution decoder:* After representing the missing sensing information via forward and backward hidden state, namely  $\Upsilon^P := [\Upsilon^{G,P}, \Upsilon^{F,P}]$ , the multi-resolution decoder must learn the distribution of the complete sensing sequence given such hidden states, i.e.,  $p(\mathbf{S}^P|\Upsilon^P)$ . This a multi-resolution decoder can handle different time scales thereby improving the *generalizability* of our prediction model with respect to the rate of change of the environment. That is, modeling different time scales, we can capture both short-term and long-term dependencies in the data, which can be important for accurate imputation. As in [25], our multi-resolution decoder performs its decoding strategy from the most coarse to the finest-grained resolutions. A decoder consisting of  $Z$  resolutions is made up of decoding functions  $f^1, \dots, f^Z$ , each of which predicts every  $\Delta_z = 2^{Z-z}$  steps. To select the missing step  $t$ , which is close to the midpoint  $\lceil \frac{(i+j)}{2} \rceil$ , the decoder

first finds two known steps  $i$  and  $j$  as pivots and, then, it determines the smallest resolution  $z$  that satisfies  $\Delta_z \leq \frac{(j-i)}{2}$ . Using the forward states  $v_i^F$  and the backward states  $v_j^B$ , the decoder updates the hidden states at time  $t^*$ . Subsequently, a decoding function  $f^z$  is applied to map the hidden states to the distribution over the outputs, denoted as  $p(S_i^{P^*} | \Upsilon^P)$ . Once an imputation round is complete, the mask  $\Xi^P$  is updated to  $[1, 1, 1]^T$  and the process proceeds to the next resolution.

3) *Imputation Approach Learning Objective*: Let  $\mathcal{S} = \mathcal{S}^*$  be the collection of the comprehensive sensing information (containing continual and uninterrupted sensing information).  $\mathcal{I}_\omega(\mathcal{S}, \Xi)$  represents our generative imputation model parametrized by  $\omega$ , and  $p(\Xi)$  is the prior over masking computed by averaging the blockage score over previous time slots. Thus, the system can be trained as follows:

$$\min_{\omega} \mathbb{E}_{\mathcal{S}^* \sim \mathcal{S}, \Xi \sim p(\Xi), \hat{\mathcal{S}} \sim \mathcal{I}(\mathcal{S}, \Xi)} \left[ \sum_{t=1}^T \mathcal{L}_{\mathcal{I}}(\hat{\mathcal{S}}_t, \mathcal{S}_t) \right], \quad \text{where} \quad \mathcal{L}_{\mathcal{I}} = \left\| \hat{\mathcal{S}}_t - \mathcal{S}_t \right\|^2.$$

Minimizing this objective function enables us to go from coarse grained sensing vectors with missing information in regards to user behavior towards fine-grained situational awareness which yields continual context in regards to the user behavior and the environmental time-varying dynamics until *present time*. Next, we discuss our forecasting system.

## B. Adversarial Transformer for Future User Behavior and Environment Forecasting

1) *Forecasting Model Architecture*: So far, we obtained a comprehensive, complete, and continual sensing information (until present time) that empowers both the network and XR application to instantaneously respond to user and environmental behaviors. To enable *proactive anticipatory intelligence*, i.e., the ability to proactively anticipate and respond to user and environmental behaviors, we propose an encoder-decoder based transformer structure and an auxiliary discriminator, as in Fig. 3, as *a forecasting system* for our continual sensing information. Encoder-decoder based transformers are known to be good for time series forecasting by virtue of their attention mechanisms in multi-head attention layers that allows the transformer to capture long-term dependencies within the continual sensing data outputted by our imputations. Similarly to the neural network layer structure of [26], the encoder and the decoder both contain an identical number of layers. Each layer consists of a multi-head self attention layer and a feed-forward network. For the transformer, given a novel architecture family of transformations, namely,  $\alpha$ -



entmax (see [27], [28]) was adopted<sup>7</sup>.

To improve the *generalizability* of our AI framework and properly characterize the stochasticity of the data, we adopt an adversarial training process. Rather than relying on minimizing likelihood or quantile loss functions, we use the adversarial training process to regularize the sensing data generated from the encoder-decoder network. By doing so, we are able to improve the robustness of our framework and better handle variations in the data. Adversarial learning here enables the framework to learn from both the observed and unobserved data, thus improving its ability to generalize to new, unseen data. Thus, per Fig. 3, a discriminator network is added to our forecasting system to improve the time-variant accuracy. Similarly to [26], the discriminator network consists of three fully connected linear layers with LeakReLU [29].

2) *Forecasting Learning Objective*: First, the goal of the discriminator is to distinguish whether the input sensing data are predicted or ground-truth values by computing the cross-entropy loss function. Here, the encoder-decoder transformer network acts as the generator  $\mathcal{G}$  whose goal is to minimize the quantile loss and adversarial loss. Henceforth, the goal of the overall forecasting system is to optimize the following objective:

$$\begin{aligned} & \arg \min_{\mathcal{G}} \max_{\mathcal{D}} \lambda_{\mathcal{A}} \mathcal{L}_{adv}(\omega^{\mathcal{G}}, \omega^{\mathcal{D}}) + \mathcal{L}_{\rho}(\omega^{\mathcal{G}}) \\ & \mathcal{L}_{adv}(\omega^{\mathcal{G}}, \omega^{\mathcal{D}}) = \mathbb{E} \left[ \log(\mathcal{D}(\mathbf{S})) \right] + \mathbb{E} \left[ \log(1 - \mathcal{D}(\hat{\mathbf{S}})) \right] \\ & \mathcal{L}_{\rho}(\omega^{\mathcal{G}}) = 2 \sum_{t=0}^{\mathcal{T}} \sum_{i=t_0+1}^{t_0+\tau} P_{\rho}(\mathbf{S}_{i,t}, \hat{\mathbf{S}}_{i,t}), \quad P_{\rho}(\mathbf{S}_{t,i}, \hat{\mathbf{S}}_{t,i}) = \Delta \mathbf{S}_{t,i} \left( \rho \mathbb{1}_{\hat{\mathbf{S}}_{t,i} > \mathbf{S}_{t,i}} - (1 - \rho) \mathbb{1}_{\hat{\mathbf{S}}_{t,i} \leq \mathbf{S}_{t,i}} \right), \end{aligned}$$

where  $\omega^{\mathcal{G}}$  and  $\omega^{\mathcal{D}}$  are the parameters of the generator and discriminator respectively,  $\mathcal{T}$  is the overall time span,  $P_{\rho}$  is the normalized quantile loss ( $\rho$ -risk),  $\Delta \mathbf{S}_{i,t} = (\hat{\mathbf{S}}_{i,t} - \mathbf{S}_{i,t})$ , and  $\lambda_{\mathcal{A}}$  is the trade-off hyperparameter between  $\mathcal{L}_{adv}$  and  $\mathcal{L}_{\rho}$ . The network is able to learn how to generate more accurate and reliable predictions by minimizing the quantile loss and adversarial loss, as well as regularizing the sensing data through the discriminator. This improves the generalizability of the overall framework by allowing it to properly account for the stochasticity of the data. Essentially, this adversarial generative approach encourages the network to learn the underlying distribution of the data, rather than simply memorizing the training data. As a result, the network can better generalize to new, unseen data, which is crucial for accurate future prediction and subsequent robust optimization.

Given the aforementioned imputation and forecasting systems, our logical next step is to feed

<sup>7</sup>In essence, sparse attention models exhibit a form inductive bias that increases focus on relevant sensing information and makes the continual sensing sequence more interpretable as a result of the causality in the user's mobility.

this information to the communication system so as to minimize the handover costs and improve the THz link resilience, as explained next.

## V. QOPE-CENTRIC AND SENSING-AWARE HANDOVER OPTIMIZATION

In this section, our goal is to leverage the comprehensive and predictive sensing information that we extracted so as to optimize the wireless XR system performance *instantaneously*. To do so, we must first define the QoPE for XR users over the reality-virtuality spectrum.

### A. QoPE of XR users

In a THz network, handover optimization, whether in indoor or outdoor settings, is paramount due to the dynamic and unpredictable nature of the environment. Essentially, THz links have a limited range, narrow beamwidth, and are sensitive to blockages (including self-blockage). Thus, while resources such as bandwidth, resource blocks, or power are important, handover has an immediate impact on the user QoPE as it directly affects the ability to maintain a LoS link [12]. Traditionally, handover schemes rely on a combination of parameters, which usually include signal-to-interference-plus-noise-ratio (SINR) thresholding, signal strength, distance, and quality-of-service (QoS) indicators. While these parameters are effective in ensuring reliable connectivity in conventional services, they fail to capture the user's perspective or their QoPE. Therefore, adopting existing handover schemes in personalized highly immersive experiences, such as XR applications, can disrupt the seamless user experience. Moreover, as narrow THz beams are susceptible to micro-mobility and micro-orientation, such handover techniques are likely to result in frequent beam interruptions and a lack of continual connectivity, negatively impacting the overall network performance. Thus, we need more sophisticated handover schemes that consider user-centric metrics and the unique THz characteristics. Consequently, to design an XR user-centric handover scheme, we must first tractably define the QoPE of XR users over the reality-virtuality continuum from AR all the way to VR.

**Definition 1:** The QoPE of an XR user is given by:

$$\beta = (\lambda_1 R_d + \lambda_2 R_w) P(\vartheta \leq \lambda_3 \vartheta_t). \quad (12)$$

Here,  $\lambda_1, \lambda_2$ , and  $\lambda_3 \in [0, 1]$ , while  $R_d$  and  $R_w$  are the downlink and uplink data rates respectively.  $\vartheta$  is the E2E delay that encompasses the transmission delay, the computing, queuing, and handover delays. To characterize this continuum, we define a parameter  $\aleph$  as the reality-virtuality

scaling factor. For fully virtual services (VR),  $\aleph = 1$ , meanwhile for services that overlay reality with augmented content (AR),  $\aleph = 0$ . Essentially, the QoPE must depend on the level of immersion in the virtual world and thus on the defined scaling factor  $\aleph$ . Hence,  $\lambda_1 - \lambda_2 \propto c\aleph$  and  $\lambda_3 \propto (1 - c\aleph)$ , where  $c$  depends on the XR generation and device requirements. For instance, for  $\aleph = 0$ ,  $\lambda_1 = \lambda_2$ , as  $\aleph$  increases, the gap between  $\lambda_1$  and  $\lambda_2$  increases. This relationship is a byproduct of the fact that, in AR a bidirectional high data rate is needed to sustain a high QoPE; meanwhile, in VR the focus is only on the downlink data rate. Furthermore, as  $\aleph$  increases from 0 to 1,  $\lambda_3$  decreases. This is because VR requires a higher level of immersiveness and haptic feedback, and thus require more stringent reliability measures. Meanwhile, AR does not require full immersion. Hence, as shown in (13), we propose a handover triggering criteria that integrates the QoPE of the user and its situational awareness. Essentially, if there exists a dynamic blocker that is getting closer to the associated user in the current/future time slot, a handover must occur.

$$\left\{ \begin{array}{ll} \mathbf{S}_{b,n,u}^N(t) \rightarrow \mathbf{S}_{b,n,u}^L(t) \wedge \text{CRLB} \leq \text{CRLB}^{\text{th}} & \text{initiate sensing-aware handover,} \\ \mathbf{S}_{b,n,u}^N(t+1) \rightarrow \mathbf{S}_{b,n,u}^L(t+1) \wedge \mathcal{L}_{\mathcal{I}} \leq \mathcal{L}_{\mathcal{I}}^{\text{th}} & \text{initiate sensing-aware proactive handover,} \\ \beta_{u,n,b}(t) < \beta_{\text{th}} & \text{initiate QoPE-centric handover,} \\ \beta_{u,n,b}(t) \geq \beta_{\text{th}} & \text{maintain the current link.} \end{array} \right. \quad (13)$$

Essentially, as shown in (13), our handover triggering scheme leverages our predicted continual and future user behavior as well as the environment dynamics so as to anticipate future beam misalignment. Furthermore, when a behavior is not anticipated our handover scheme instantaneously gets triggered when the QoPE of the user drops. This enables a *resilient* [30] decision making mechanism that can flexibly interact with the environment regardless of its dynamics and the accuracy of our estimated and predicted sensing parameters.

Although our handover process is sophisticated, the XR user experience can still be slightly degraded during this time, especially when a handover occurs due to QoPE drops. To ensure optimal performance, our network optimization framework must discourage frequent handovers that increase E2E delay and impact QoPE. Therefore, we propose a user-centric handover cost and the total number of handovers per meter for a user  $u$  as follows:

$$\varrho_u = \min(h_u v_u \vartheta_u^h, 1), \quad h_u = \frac{\sum_{n \in \mathcal{N}} \sum_{b \in \mathcal{B}} \{P[x_{b,n,u}(t)x_{b,n,u}(t-1) = 0]\}}{D_u}, \quad (14)$$

where  $x_{b,n,u} = 1$ , if user  $u$  is associated to subarray  $n$  of RIS  $b$ , and  $x_{b,n,u} = 0$  otherwise,  $v_u$  is the velocity of XR user  $u$ ,  $D_u$  is the total distance traveled by user  $u$ , and  $\vartheta_u^h$  is the handover time delay.

### B. Handover Optimization and User Association Problem Formulation

To guarantee a seamless experience to each and every XR user simultaneously, our goal is to minimize the handover cost defined in (14), while guaranteeing a high QoPE for every single user instantaneously. This optimization must also be cognizant of the estimated sensing parameters and their corresponding errors. In essence, performing handover based on erroneous sensing information will jeopardize the network performance. Hence, we first define the collective utility of all the active subarrays as follows:

$$G(\mathbf{x}) = \lim_{T \rightarrow \infty} \sum_t \sum_{u \in \mathcal{U}} \sum_{n \in \mathcal{N}} \sum_{b \in \mathcal{B}} x_{b,n,u}(t) \beta_{u,n,b}(t) \times (1 - \varrho(t)). \quad (15)$$

The goal of the RISs is to find optimal handover strategies that maximize the collective team utility. Let  $\pi_{b,n}(x_{b,u,n}(t)|x_{b,u,n}(t-1), \mathbf{S}_{b,n,u}^L(t, t+1), \mathbf{S}_{b,n,u}^N(t, t+1))$  be the strategy of subarray  $n$  in RIS  $b$  that is defined as the probability that the considered subarray serves user  $u$  at time  $t$ , after successfully serving user  $u$  at  $t-1$ . This probability is further conditioned on the available QoPE  $\beta_{u,n,b}(t)$  and the situational awareness of the current and future time slots  $\mathbf{S}_{b,n}^L(t, t+1)$  and  $\mathbf{S}_{b,n}^N(t, t+1)$ . As such, the expected collective utility is given by:

$$\bar{G}(\boldsymbol{\pi}) = \sum_{\mathbf{x} \in \mathcal{X}} G(\mathbf{x}) \prod_{b \in \mathcal{B}} \prod_{n \in \mathcal{N}} \prod_{u \in \mathcal{U}} \pi_{b,n}(x_{b,u,n}(t)|x_{b,u,n}(t-1), \beta_{u,n,b}(t), \mathbf{S}^L(t, t+1), \mathbf{S}^N(t, t+1)),$$

where  $\mathcal{X}$  is the set of all possible associations that subarray  $n$  of RIS  $b$  can perform at time  $t$ . We seek to find a handover policy that optimizes the data rate, continuity, and robustness over all the active THz links of the RISs's subarrays. We thus, formulate the handover and user association problem of an RIS-assisted THz indoor network serving XR users:

$$\max_{\boldsymbol{\pi} = \{\pi_1, \dots, \pi_{B \times N}\}} \bar{G}(\boldsymbol{\pi}), \quad (16a)$$

$$\text{s.t. } \lambda_1 R_{d,u}(t) + \lambda_2 R_{w,u}(t) \leq \lambda_1 R_d^{th}(t) + \lambda_2 R_w^{th}(t), \forall t \in (0, \infty), \forall u \in \mathcal{U}, \quad (16b)$$

$$P(\vartheta(t) \leq \lambda_3 \vartheta_{th}) \geq \gamma_{th, \mathbb{R}}, \forall u \in \mathcal{U}, \quad (16c)$$

$$\sum_{\mathbf{x} \in \mathcal{X}} \prod_{b \in \mathcal{B}} \prod_{n \in \mathcal{N}} \prod_{u \in \mathcal{U}} \pi_{b,n}(x_{b,u,n}(t)|x_{b,u,n}(t-1), \beta_{u,n,b}(t), \mathbf{S}^L(t, t+1), \mathbf{S}^N(t, t+1)) = 1, \quad (16d)$$

$$0 \leq \pi_{b,n}(x_{b,u,n}(t)|x_{b,u,n}(t-1), \beta_{u,n,b}(t), \mathbf{S}^L(t, t+1), \mathbf{S}^N(t, t+1)) \leq 1. \quad (16e)$$

(16a) maximizes the time average of QoPE of active users associated to subarrays, while taking into account the handover cost. (16b) and (16c) take into account each user's downlink/uplink data rate and reliability explicitly. (16b) is the downlink/uplink condition that guarantees the satisfaction of the rate requirement based on the type of XR service on the virtuality-reality

spectrum. Similarly, (16c) is the reliability condition that guarantees that the E2E delay is less than a desired threshold. This E2E delay considers the computing, queuing, transmission, and handover latency. (16d) and (16e) are feasibility conditions. From (16), one observes that the objective function is non-convex. Furthermore, (16a) exhibits multiple inter-dependent and correlated parameters such as the QoPE, the E2E delay, and the handover cost. Additionally, the binary association decision variable  $x_{b,n,u}$  makes this problem difficult to solve via vanilla non-convex optimization frameworks. Optimally solving this problem, i.e., guaranteeing bidirectional rate, reliability, and low latency for all XR simultaneously and instantaneously requires imposing restrictions or assumption on mobility, blockage, or the sensed environment. However, making such assumptions would not provide an accurate representation of the dynamic behavior of the THz network and the way in which XR users interact with it. Consequently, to address the highly varying, dynamic, and non-stationary nature of the THz channel and XR user behavior, we propose a novel semi-distributed multi-agent RL framework that can fulfill the personal requirements of individual users while shrinking the gap between the best-case and worst-case performance. This framework enables agents to learn from their experiences, from the predicted and forecasted sensing information in Section IV, and adapt their decision-making process based on the current/future network conditions and user requirements, resulting in a more efficient, resilient, and personalized performance.

### *C. Semi-Distributed Multi-Agent RL for Robust Handover Optimization*

Given that the goal of (16) is to deliver a user-centric QoPE, it cannot be solved through a fully centralized approach where a central server makes handover decisions without considering the specific needs of individual users. Due to the highly dynamic and non-stationary nature of the THz channel and the diverse needs of individual users, achieving instantaneous reliability for all users at all times is challenging. We adopt a resilient and robust approach in our optimization solution to address the inherent uncertainties and variations in the system. Instead of solely focusing on maximizing the QoPE or reliability, we aim to find mechanisms that enable a quick rebound from occasional dips in performance. By adopting such an approach, we ensure that the system remains adaptable and can function optimally under varying conditions and scenarios. Consequently, we propose a novel semi-distributed multi-agent RL framework that brainstorms collaboratively yet executes individually. That is to address individual user's complex time varying requirements, every subarray will have its own neural network to prioritize decision-

making for its tagged user. To account for the welfare of the overall network, a centralized feedback characterizing the QoPE of all other users, will be communicated from the central mobile edge computing (MEC) server to the reward of each subarray and its tagged user. Thus, guaranteeing the maximization of the collective utility in (16a).

In fact, the main goal when solving (16) is to find a policy for each subarray that can maximize the individual QoPE requirements of its associated XR user given the available sensing information, while maximizing the collective utility, i.e., focusing on individual QoPE while not overshadowing the collective performance. Furthermore, the obtained continual and future sensing information may be erroneous and do not always reflect the ground truth of each subarray. That is, in (13), we can see that the handover process is a function of the accuracy of estimations and predictions, thus our environment is *partially observable*. We next introduce the components of our semi-distributed multi-agent RL framework:

- *Agents*: The agents are the subarrays in  $\mathcal{N}$  of all the RIS-operated RISs in  $\mathcal{B}$ .
- *Observations*: To ensure fair collaboration among subarrays, each agent observes its sensing information, the QoPE of its user, and the sum of QoPE of all active users<sup>8</sup>. Thus,  $\mathbf{o}_{b,n,u}(t) = [x_{b,n,u}(t-1), \mathbf{S}^L(t, t+1), \mathbf{S}^N(t, t+1), \beta_{u,n,b}(t), \sum_{b \in \mathcal{B}} \sum_{n \in \mathcal{N}} \sum_{i \neq u \in \mathcal{U}} x_{b,u,n}(t) \beta_{u,n,b}(t), \rho_u]$ . The set of observations of all the subarrays of all the RISs is  $\mathcal{O} = \{\mathbf{O}_0, \mathbf{O}_1, \dots, \mathbf{O}_t\}$ , where  $\mathbf{O}_t = [o_{1,1}^t, \dots, o_{B,N}^t]$  are the states of the subarrays at time step  $t$ . This enables each subarray to make a decision based on its locally available measurements as well as the previous association performed.
- *Action*: The action of each agent is to perform a handover decision or to maintain the currently active link. This decision requires modifying  $x_{b,n,u}(t)$ 's binary value and adjusting the beam of the considered subarray to the new or currently associated user, based on their tracking information in  $\mathbf{S}^L(t), \mathbf{S}^N(t)$ . These actions are given by  $\mathbf{a}_t = [a_{1,1}(t), \dots, a_{B,N}(t)] \in \mathcal{A}$ .
- *Strategies*: The strategy of each subarray is the handover and user association strategy in (16).
- *History*: The history of each agent is defined as the set of all measurements, observations, and actions collected up to time  $t$  so as to enable each learning agent opportunistically learn the time-varying nature of the policy.  $\mathcal{H}_{b,n}(t) = \{a_{b,n}(t), x_{b,n,u}(t-1), \mathbf{S}^L(t, t +$

<sup>8</sup>Such observations can be made available by measuring the uplink/downlink sum rates at the RIS-operated BSs, and by performing a ping that enables measuring the E2E delay and reliability.

1),  $\mathbf{S}^N(t, t+1), \beta_{u,n,b}(t), \sum_{i \neq u \in \mathcal{U}} \beta_{u,n,b}(t), \rho_u\}$ . Here, it is important to note that while each subarray takes actions following its own user-centric strategy, from an RL perspective, one might think they are unaware of the actions being made from other user equipments (UEs). That said,  $\mathbf{S}^L(t, t+1)$  provides a local situational awareness of the surrounding blockers as well as a future prediction of this local area. In other words, each agent is only cognizant of the actions of other agents that may affect them. The centralized feedback  $\sum_{b \in \mathcal{B}} \sum_{n \in \mathcal{N}} \sum_{i \neq u \in \mathcal{U}} x_{b,u,n}(t) \beta_{u,n,b}(t)$  enables weighing each agent's contribution to the total welfare of the network.

- *Reward*: The reward of our system is designed in a semi-distributed fashion. That is, the reward of each subarray must measure the benefit of a selected action on: a) its current, established link, and b) the effect of the action on the overall network's robustness and resilience. Thus, we have:  $r_{b,n}(t) = x_{b,n,u}(t) \beta_{u,n,b}(t) \times (1 - \varrho_{b,n,u}(t)) + \zeta_{b,n} \sum_{i \neq u \in \mathcal{U}} \sum_{n \in \mathcal{N}} \sum_{b \in \mathcal{B}} x_{b,n,u}(t) \beta_{u,n,b}(t)$ , where  $\zeta_{b,n} \in (0, 1)$  that can be tuned based on factors such as the a) the density of users in the network, b) the carrier frequency and the corresponding beamwidth, c) the level of cooperation needed to achieve desirable results. The accumulated discounted reward can be given by  $R_{b,n}(t) = \sum_{t'=t}^T \gamma^{t'-t} r_{b,n}(t)$  where  $\gamma$  is the discount factor. This accumulated reward exemplifies maximizing the collective utility in (16a) in an individualistic and instantaneous way that can still improve the collective performance. Here,  $\gamma = 0$  amplifies the current instantaneous performance only, while ignoring any lessons that can be leveraged from previous handover policy. Meanwhile,  $\gamma = 1$  would average out the return. Note that, the optimal objective of maximizing the user's instantaneous QoPE requires incorporating past handover policies and user associations, which is why setting  $\gamma = 0$  would result in a suboptimal learning process.

To address the time-varying and non-stationarity nature of the THz network as well as the complexity of the multi-agent partially observable process, every agent or subarray adopts a hysteretic deep recurrent Q-network [31], [32]. In essence, each subarray  $n$  acts as quasi-independent learner (not fully independent as the centralized feedback depends on other agents) and maintains its own hysteretic deep recurrent Q-network. In contrast to overly-optimistic multi-agent RL frameworks like vanilla distributed deep Q-learning, which tend to overlook low returns caused by teammates' exploratory actions and subsequently result in significant overestimation of Q-values in stochastic environments, hysteretic deep recurrent Q-networks can discern that low

returns may stem from environmental stochasticity and should not be disregarded. This approach is particularly crucial for optimizing THz networks, which are susceptible to extreme events like sudden blockages and molecular absorption, as well as micro-mobility and micro-orientation changes. By taking the dynamic and unpredictable nature of the environment into account, this approach allows for improved adaptation and optimization, ensuring that the reliability of the system is maintained and quickly restored following intermittent THz links. This is particularly crucial in providing uninterrupted and dependable service for XR users, whose needs may change over time, and guarantees a resilient user experience that can promptly recover from any disruptions. Moreover, the semi-distributed learning framework used in this approach ensures guaranteed convergence due to the adoption of asynchronous updates, where agents update their policy and value function independently and asynchronously. Although the optimality of the solution may not be guaranteed in highly dynamic and non-stationary environments like THz networks, the quick adaptation of deep hysteretic networks enables the system to maintain robust and resilient performance in response to unpredictable user behavior. Hysteretic deep recurrent Q-networks leverage two distinct learning rates to handle the complex dynamics of the learning process. The first learning rate,  $\eta_1$ , is used when the temporal difference (TD)-error is non-negative. In contrast, the second learning rate,  $\eta_2$ , is much smaller and is utilized to slow down the degradation of Q-values associated with previously positive experiences resulting from successful operations [31]. By implementing this approach, hysteresis is introduced, allowing subarrays to be more resilient against negative learning, exploration, and concurrent actions. This approach significantly improves the stability and robustness of the learning process, leading to better overall performance and expedited convergence.

Similarly to [32], the deep hysteretic Q-network adopted is with one input layer, two fully connected hidden layers, one RNN hidden layer, a dueling layer, and an output layer. The subarray's local observations and the estimated state-action value  $Q_{b,n}$ , respectively define the input and output layer of the hysteretic deep recurrent Q-network. Multi-agent RL frameworks are known to face the challenge of *shadowed equilibria*, a phenomenon where local observations and non-stationarity cause locally optimal actions to become suboptimal at the global level [33]. Addressing this challenge effectively and stabilizing the learning process is crucial. To ensure a resilient policy for each subarray and enable a smooth recovery from sudden disruptions of THz links, we stabilize the learning process using a synchronized sampling strategy known as concurrent experience replay trajectories [31].



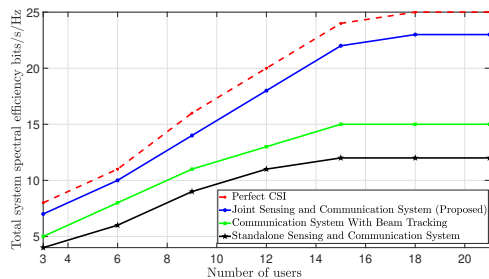


Fig. 4: Spectral efficiency versus number of users.

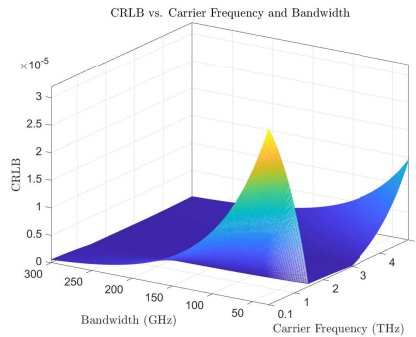
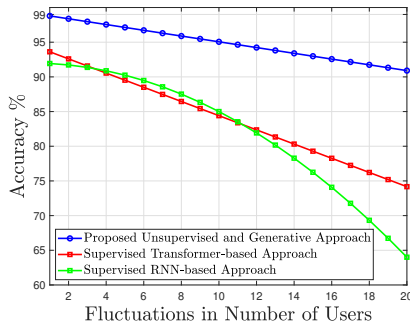
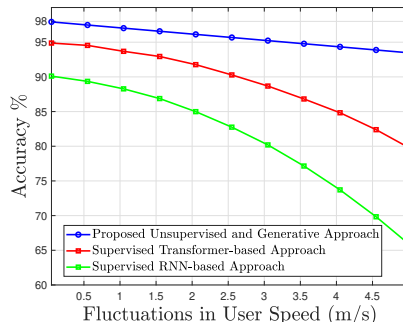


Fig. 5: CRLB versus carrier frequency (THz) and bandwidth (GHz).



(a)



(b)

Fig. 6: Generalizability of our integrated imputation and forecasting system with respect to (a) Fluctuations in the number of users in/out of the indoor area, and (b) Fluctuations in user's speed (m/s).

## VI. SIMULATION RESULTS AND ANALYSIS

For our simulations, we consider an indoor area modeled as a square of size  $24\text{ m} \times 24\text{ m}$  whereby the RISs are deployed over its three walls. The molecular absorption was obtained from the sub-THz model in [34] with 1% of water vapor molecules. We set:  $N = 64$  antennas,  $Q = 32$  antennas,  $f = 0.275\text{ THz}$ ,  $W = 10\text{ GHz}$  (unless stated otherwise), and  $p = 30\text{ dBm}$ . All statistical results are averaged over a large number of independent runs. For AR, we set  $\lambda_1 = 1$ ,  $\lambda_2 = 1$ , and  $\lambda_3 = 1$ . For VR, we set  $\lambda_1 = 1$ ,  $\lambda_2 = 0.6$ , and  $\lambda_3 = 0.8$ , and, finally for MR, we let  $\lambda_1 = 0.9$ ,  $\lambda_2 = 0.9$ , and  $\lambda_3 = 0.95$ . The reliability threshold set  $\nu_t = 24\text{ ms}$ . VR services ensure the immersion in a virtual world by guaranteeing the a QoPE below the 20 ms as  $\lambda_3 = 0.8$  for VR. The network was simulated with data generated from XR users moving according to a random walk scheme as well as a WiFi positioning dataset [35] so as to have a general scheme for user mobility.

In Fig. 4, the total spectral efficiency defined as in [36] is shown. Fig. 4 clearly shows the benefits of deploying a joint sensing and communication system that shares hardware, waveform,

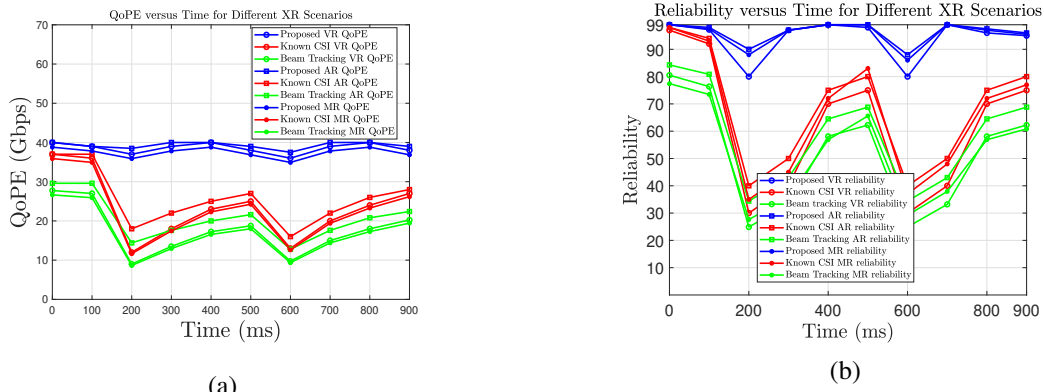


Fig. 7: (a) QoPE of XR users versus XR session time, (b) Reliability of XR users versus XR session time.

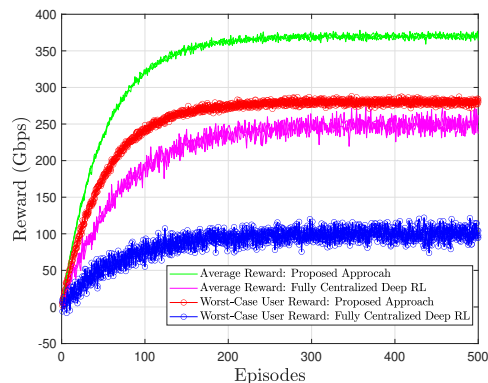


Fig. 8: Reward versus online training episodes

and spectrum. In fact, our proposed joint sensing and communication approach achieves a 42% and 75% improvement respectively compared to a communication system with beam training and a standalone sensing and communication system. Fig. 5 showcases the effect of varying the bandwidth and the carrier frequency on the CRLB. We can see that as intuitively expected, higher bandwidths minimize the CRLB, nonetheless, the CRLB's behavior versus carrier frequencies is not monotonic. In fact, we can see that the CRLB decreases for carrier frequencies in the range of 0.1 THz – 1 THz. Nonetheless, for higher carrier frequency ranges, Fig. 5 shows that the CRLB starts to increase again due to the effect of more significant molecular absorption lines. From Fig. 5, we also observe that increasing the bandwidth at such high carrier frequencies (1 THz – 5 THz) can also enable decreasing the CRLB.

In Fig. 6, the generalizability of our joint imputation and forecasting system is evaluated versus fluctuations and new unseen user behavior (which are new mobility patterns tuned in this testing period). We compare our approach to RNN-based and transformer-based approaches which are well known models for predicting temporal dynamics [37]. From Fig. 6, we observe that, when

increasing the fluctuations in the number of users as well as the users speed, the accuracy of our proposed scheme remains high. Meanwhile, deep learning learning schemes relying on datasets and having a bias cannot adapt to fluctuations properly. Their accuracy decreases rapidly as such fluctuations and unseen behavior pattern increases.

In Fig. 7a, the QoPE of an XR user (over different XR scenarios on the continuum) is evaluated. We compare our proposed approach with communication-only schemes that use known CSI and beam tracking so as to study the potential benefits of joint sensing and AI-driven situational awareness in enhancing communication system. First, we observe that maintaining a high AR QoPE is much easier than MR and VR. The difference in QoPE increases because of extreme events such as blockages around time 200 ms and 600 ms. Fig. 7a shows that our proposed approach is able to recover easily from blockages and thereby demonstrating a *high resilience*. This is by virtue of the network optimization design as well as the knowledge of future time slots. Meanwhile, for communication only schemes with known CSI and beam tracking, the time needed to recover from such extreme events is much longer (by 270 ms). In fact, by virtue of our semi-distributed, sensing-aware, and QoPE-centric approach, our proposed approach achieves gains of 60.27% and 110% when compared to known CSI and beam tracking schemes respectively. We observe a similar behavior for the reliability in Fig. 7b. Indeed, the reliability of VR (compared to AR and MR) is more difficult to maintain, as it requires a more stringent E2E delay bound. Furthermore, similar to the QoPE we can see that the reliability of the system takes time to recover from disruption in links in the known CSI and beam tracking schemes. Fig. 7b shows that, our proposed approach achieves 61% and 78% gains in the reliability compared to known CSI and beam tracking schemes.

In Fig. 8, the average reward and the worst-case user reward of our proposed approach are evaluated and compared to fully centralized deep RL schemes. From Fig. 8, we observe that, for the average and the worst-case user, our semi-distributed deep Q hysteretic RL scheme achieves higher rewards than fully a centralized deep RL schemes. In fact, we can see that the worst-case reward of our proposed approach is higher than the average-reward of centralized deep RL schemes. When comparing with centralized vanilla deep RL frameworks, we observe a 1.5-fold improvement in the average reward and a two-fold improvement in the worst-case reward.

## VII. CONCLUSION

In this paper, we have proposed a novel joint sensing, communication, and AI approach for achieving optimized and resilient wireless XR experiences at THz bands. We leverage THz-

operated RISs as base stations to extract sensing parameters by opportunistically utilizing uplink communication waveforms. Our framework comprises a tensor decomposition framework, a non-autoregressive multi-resolution generative AI framework with an adversarial transformer, and a QoPE-centric and sensing-driven optimization that uses a semi-distributed multi-agent deep recurrent hysteretic Q-neural network. Our goal is to maximize individual QoPEs and improve the robustness and resilience of THz links. Through our analysis and simulations, we have concluded the following observations:

- Deploying THz base stations at carrier frequencies higher than 1 THz is challenging in the sensing and communication realm. Although such bands may offer high bandwidths for high-resolution sensing and data rates, our results show that the possibility of performing erroneous sensing estimates increases due to molecular absorption lines. Hence, there is a need for open problems that enable higher rates at the sub-THz spectrum [3].
- Ensuring an instantaneous reliability of five nines with THz frequencies alone remains challenging even with sensing. However, by combining sensing and AI, we can better control future networks and make them more robust and resilient. Further research is needed to explore the impact of joint sensing, communication, and AI in a multi-band scheme that integrates sub-6 GHz, millimeter wave (mmWave), and THz frequencies to achieve resilient five nines reliabilities and high quality of personalized experience.
- Novel intelligence-centric metrics similar to the QoPE should be proposed to ensure the requirements of future 6G and beyond applications are met. The resilience of certain application metrics must be evaluated with respect to time, specifically how quickly they rebound to their acceptable range. This is especially important for future 6G applications that require instantaneous performance.

## APPENDIX

### A. Proof of Theorem 1

Problem (6) can be solved efficiently by the alternating least squares matrix factorization procedure [38]. Since we deal with a third order tensor, this factorization has three iterative steps. Then, it fixes two factor matrices and minimizes the error with respect to the considered factor matrix as:

$$\tilde{\mathbf{A}}^{(t+1)} = \arg \min_{\tilde{\mathbf{A}}} \left\| \mathbf{Y}_{n,(1)}^T - \left( \tilde{\mathbf{C}}^{(t)} \odot \tilde{\mathbf{B}}^{(t)} \right) \tilde{\mathbf{A}}^T \right\|_F^2, \quad \tilde{\mathbf{B}}^{(t+1)} = \arg \min_{\tilde{\mathbf{B}}} \left\| \mathbf{Y}_{n,(2)}^T - \left( \tilde{\mathbf{C}}^{(t)} \odot \tilde{\mathbf{A}}^{(t+1)} \right) \tilde{\mathbf{B}}^T \right\|_F^2,$$

$$\tilde{\mathbf{C}}^{(t+1)} = \arg \min_{\tilde{\mathbf{C}}} \left\| \mathbf{Y}_{n,(3)}^T - \left( \tilde{\mathbf{B}}^{(t+1)} \odot \tilde{\mathbf{A}}^{(t+1)} \right) \tilde{\mathbf{C}}^T \right\|_F^2, \quad (17)$$

where,  $\odot$  is the Khatri-Rao product symbol. The exact factor matrices are related to their estimates according to:  $\tilde{\mathbf{A}} = \mathbf{A}\mathbf{J}_1\mathbf{\Gamma} + \mathbf{E}_1$ ,  $\tilde{\mathbf{B}} = \mathbf{B}\mathbf{J}_2\mathbf{\Gamma} + \mathbf{E}_2$ ,  $\tilde{\mathbf{C}} = \mathbf{C}\mathbf{J}_3\mathbf{\Gamma} + \mathbf{E}_3$ , where  $\{\mathbf{J}_1, \mathbf{J}_2, \mathbf{J}_3\}$  are unknown nonsingular diagonal matrices that satisfy  $\mathbf{J}_1\mathbf{J}_2\mathbf{J}_3 = \mathbf{I}$ ,  $\mathbf{\Gamma}$  is an unknown permutation matrix, and  $\{\mathbf{E}_1, \mathbf{E}_2, \mathbf{E}_3\}$  are estimation error matrices. By applying a maximum likelihood estimator on each one of the equations and assuming that the estimation error matrices  $\{\mathbf{E}_1, \mathbf{E}_2, \mathbf{E}_3\}$  follow an independently and identically distributed (i.i.d.) circularly symmetric Gaussian distribution [23], we obtain (7), (8), and (9).

### B. Proof of Lemma 1

Proving the uniqueness of our sensing parameters requires proving that the CP decomposition of  $\chi$  is unique under mild conditions with scaling and permutation ambiguities. In essence, the Kruskal's condition [21], [39] guarantee the CP decomposition if the following condition is met:  $k_A + k_B + k_C \geq 2P + 2$ , where  $k_A$ ,  $k_B$ , and  $k_C$  are the Kruskal ranks of matrices  $\mathbf{A}$ ,  $\mathbf{B}$ ,  $\mathbf{C}$  and  $P$  is the number of THz links. In fact, the Kruskal-rank of a matrix is defined the maximum number of any linearly independent columns that can be identified in a matrix. Based on [21],  $k_A$  and  $k_B$  also denote the upper bound on the maximum number of links that can be distinguished. Hence, when this upper bound condition is satisfied, one can write the Kruskal-rank of the matrices  $\mathbf{A}$ ,  $\mathbf{B}$ ,  $\mathbf{C}$ :  $k_A = \min(J, P)$ ,  $k_B = \min(T, P)$ ,  $k_C = \min(K, P)$ . As we are operating in the THz frequencies, the number of links available is quite limited, primarily restricted to either LoS or NLoS. However, the number of antennas and subcarriers at our disposal is significantly large. Consequently, the Kruskal condition is fulfilled, which ensures the uniqueness of our solution.

## REFERENCES

- [1] W. Saad, M. Bennis, and M. Chen, "A vision of 6G wireless systems: Applications, trends, technologies, and open research problems," *IEEE network*, vol. 34, no. 3, pp. 134–142, Oct. 2020.
- [2] H. Sameddeen, M.-S. Alouini, and T. Y. Al-Naffouri, "An overview of signal processing techniques for terahertz communications," *Proceedings of the IEEE*, vol. 109, no. 10, pp. 1628–1665, Aug. 2021.
- [3] C. Chaccour, M. N. Soorki, W. Saad, M. Bennis, P. Popovski, and M. Debbah, "Seven defining features of terahertz (THz) wireless systems: A fellowship of communication and sensing," *IEEE Communications Surveys & Tutorials*, vol. 24, no. 2, pp. 967–993, 2022.
- [4] A. Bazzi and M. Chafii, "Robust integrated sensing and communication beamforming for dual-functional radar and communications: Method and insights," *arXiv preprint arXiv:2303.07652*, 2023.
- [5] J. Zuo and Y. Liu, "Reconfigurable intelligent surface assisted noma empowered integrated sensing and communication," in *Proc. of IEEE Globecom Workshops (GC Wkshps)*, Rio De Janeiro, Brazil, Dec. 2022, pp. 1028–1033.
- [6] A. Guerra, F. Guidi, D. Dardari, and P. M. Djurić, "Real-time learning for THz radar mapping and uav control," in *Proc. of IEEE International Conference on Autonomous Systems (ICAS)*, Montreal, QC, Canada, Aug 2021, pp. 1–5.
- [7] W. Chen, L. Li, Z. Chen, T. Quek, and S. Li, "Enhancing THz/mmWave network beam alignment with integrated sensing and communication," *IEEE Communications Letters*, vol. 26, no. 7, pp. 1698–1702, Apr. 2022.
- [8] W. Chen, L. Li, Z. Chen, B. Ning, G. Wang, and T. Quek, "An ISAC-based beam alignment approach for enhancing terahertz network coverage," *arXiv preprint arXiv:2212.01728*, 2022.
- [9] C. Chaccour, W. Saad, O. Semiari, M. Bennis, and P. Popovski, "Joint sensing and communication for situational awareness in wireless THz systems," in *Proc. of IEEE International Conference on Communications (ICC)*, Seoul, South Korea, May 2022.

- [10] A. Faisal, H. Sarieddeen, H. Dahrouj, T. Y. Al-Naffouri, and M.-S. Alouini, "Ultramassive MIMO systems at terahertz bands: Prospects and challenges," *IEEE Vehicular Technology Magazine*, vol. 15, no. 4, pp. 33–42, Oct. 2020.
- [11] A.-A. A. Boulogeorgos and A. Alexiou, "Performance evaluation of the initial access procedure in wireless THz systems," in *Proc. of the 16th International Symposium on Wireless Communication Systems (ISWCS)*, Oulu, Finland, Aug. 2019, pp. 422–426.
- [12] C. Chaccour, M. N. Soorki, W. Saad, M. Bennis, and P. Popovski, "Can terahertz provide high-rate reliable low-latency communications for wireless VR?" *IEEE Internet of Things Journal*, vol. 9, no. 12, pp. 9712–9729, Jan. 2022.
- [13] A. Moldovan, M. A. Ruder, I. F. Akyildiz, and W. H. Gerstacker, "LOS and NLOS channel modeling for terahertz wireless communication with scattered rays," in *Proc. of IEEE Globecom Workshops (GC Wkshps)*, pp. 388–392.
- [14] R. Mendrzik, F. Meyer, G. Bauch, and M. Z. Win, "Enabling situational awareness in millimeter wave massive MIMO systems," *IEEE Journal of Selected Topics in Signal Processing*, vol. 13, no. 5, pp. 1196–1211, Aug. 2019.
- [15] C. D. Ozkaptan, E. Ekici, O. Altintas, and C.-H. Wang, "OFDM pilot-based radar for joint vehicular communication and radar systems," in *Proc. of IEEE Vehicular Networking Conference (VNC)*, Taipei, Taiwan, Dec. 2018, pp. 1–8.
- [16] A. Guerra, F. Guidi, D. Dardari, and P. M. Djuric, "Near-field tracking with large antenna arrays: Fundamental limits and practical algorithms," *arXiv preprint arXiv:2102.05890*, 2021.
- [17] G. Zhu, K. Huang, V. K. Lau, B. Xia, X. Li, and S. Zhang, "Hybrid beamforming via the kronecker decomposition for the millimeter-wave massive MIMO systems," *IEEE Journal on Selected Areas in Communications*, vol. 35, no. 9, pp. 2097–2114, Jun. 2017.
- [18] M. H. Gruber, "Statistical digital signal processing and modeling," pp. 335–336, 1997.
- [19] A. Abdallah, A. Celik, M. M. Mansour, and A. M. Eltawil, "Ris-aided mmwave mimo channel estimation using deep learning and compressive sensing," *IEEE Transactions on Wireless Communications*, Nov. 2022.
- [20] S. M. Kay, *Fundamentals of statistical signal processing: estimation theory*. Prentice-Hall, Inc., 1993.
- [21] J. B. Kruskal, "Three-way arrays: rank and uniqueness of trilinear decompositions, with application to arithmetic complexity and statistics," *Linear Algebra and Its Applications*, vol. 18, no. 2, pp. 95–138, 1977.
- [22] P. Tichavsky, A. H. Phan, and Z. Koldovsky, "Cramér-Rao-Induced Bounds for CANDECOMP/PARAFAC Tensor Decomposition," *IEEE Transactions on Signal Processing*, vol. 61, no. 8, pp. 1986–1997, Feb. 2013.
- [23] Z. Zhou, J. Fang, L. Yang, H. Li, Z. Chen, and R. S. Blum, "Low-rank tensor decomposition-aided channel estimation for millimeter wave MIMO-OFDM systems," *IEEE Journal on Selected Areas in Communications*, vol. 35, no. 7, pp. 1524–1538, Apr. 2017.
- [24] X. Liu and N. Sidiropoulos, "Cramer-rao lower bounds for low-rank decomposition of multidimensional arrays," *IEEE Transactions on Signal Processing*, vol. 49, no. 9, pp. 2074–2086, Sep. 2001.
- [25] Y. Liu, R. Yu, S. Zheng, E. Zhan, and Y. Yue, "Naomi: Non-autoregressive multiresolution sequence imputation," in *Proc. of the 33rd conference on NeurIPS*, Vancouver, Canada, Dec. 2019.
- [26] S. Wu, X. Xiao, Q. Ding, P. Zhao, Y. Wei, and J. Huang, "Adversarial sparse transformer for time series forecasting," vol. 33, Vancouver, Canada, Dec. 2020, pp. 17 105–17 115.
- [27] B. Peters, V. Niculae, and A. F. Martins, "Sparse sequence-to-sequence models," *arXiv preprint arXiv:1905.05702*, 2019.
- [28] M. Blondel, A. Martins, and V. Niculae, "Learning classifiers with fenchel-young losses: Generalized entropies, margins, and algorithms," in *Proc. of the 22nd International Conference on Artificial Intelligence and Statistics*, Naha Okinawa, Japan, Apr. 2019, pp. 606–615.
- [29] B. Xu, N. Wang, T. Chen, and M. Li, "Empirical evaluation of rectified activations in convolutional network," *arXiv preprint arXiv:1505.00853*, 2015.
- [30] R.-J. Reifert, M. Krawczyk-Becker, L. Prenzel, S. Pavlichkov, M. A. Khatib, S. A. Hiremath, M. Al-Askary, N. Bajcinca, S. Steinhorst, and A. Sezgin, "Toward resilience in mixed critical industrial control systems: A multi-disciplinary view," *IEEE Access*, vol. 10, pp. 124 563–124 581, Nov. 2022.
- [31] S. Omidshafiei, J. Papis, C. Amato, J. P. How, and J. Vian, "Deep decentralized multi-task multi-agent reinforcement learning under partial observability," in *Proc. of the 34th International Conference on Machine Learning*, Sydney, Australia, Apr. 2017, pp. 2681–2690.
- [32] M. Sana, A. De Domenico, W. Yu, Y. Lohanen, and E. C. Strinati, "Multi-agent reinforcement learning for adaptive user association in dynamic mmwave networks," *IEEE Transactions on Wireless Communications*, vol. 19, no. 10, pp. 6520–6534, Jun. 2020.
- [33] N. Fulda and D. Ventura, "Predicting and preventing coordination problems in cooperative q-learning systems," in *Proceedings of the 20th International Joint Conference on Artificial Intelligence*, San Francisco, CA, USA, Jan. 2007, p. 780–785.
- [34] J. Kokkonen, J. Lehtomäki, and M. Juntti, "A line-of-sight channel model for the 100–450 gigahertz frequency band," *EURASIP Journal on Wireless Communications and Networking*, vol. 2021, no. 1, pp. 1–15, Apr. 2021.
- [35] I. Ashraf, S. Din, S. Hur, and Y. Park, "Wi-fi positioning dataset with multiusers and multidevices considering spatio-temporal variations," *CMC-Computers Materials & Continua*, vol. 70, no. 3, pp. 5213–5232, Apr. 2021.
- [36] A. R. Chiriyath, B. Paul, and D. W. Bliss, "Radar-communications convergence: Coexistence, cooperation, and co-design," *IEEE Transactions on Cognitive Communications and Networking*, vol. 3, no. 1, pp. 1–12, Feb. 2017.
- [37] Y. Li, X. Lu, H. Xiong, J. Tang, J. Su, B. Jin, and D. Dou, "Towards long-term time-series forecasting: Feature, pattern, and distribution," *arXiv preprint arXiv:2301.02068*, 2023.
- [38] N. D. Sidiropoulos, L. De Lathauwer, X. Fu, K. Huang, E. E. Papalexakis, and C. Faloutsos, "Tensor decomposition for signal processing and machine learning," *IEEE Transactions on Signal Processing*, vol. 65, no. 13, pp. 3551–3582, Apr. 2017.
- [39] A. Bhaskara, M. Charikar, and A. Vijayaraghavan, "Uniqueness of tensor decompositions with applications to polynomial identifiability," in *Proceedings of the 27th Conference on Learning Theory*, Jun. 2014, pp. 742–778.